Limnol. Oceanogr., 53(5, part 2), 2008, 2237–2250

Mapping the spatial variability of plankton metabolism using nitrate and oxygen sensors on an autonomous underwater vehicle

Kenneth S. Johnson and Joseph A. Needoba[1]
Monterey Bay Aquarium Research Institute, 7700 Sandholdt Road, Moss Landing, California 95039

Abstract

It is now possible to make highly resolved vertical (<1 m) and horizontal (3 m at constant depth and ~400 m when undulating from surface to 100 m) measurements of nitrate concentration in the upper ocean using sensors deployed on propeller-driven autonomous underwater vehicles (AUVs). The ability to make such highly resolved measurements opens the possibility of detecting small-scale anomalies in nutrient fields that are created by locally high rates of primary production. We employed an in situ ultraviolet spectrophotometer optical nitrate sensor and Sea-Bird oxygen sensor mounted on the Monterey Bay Aquarium Research Institute Dorado AUV to investigate the spatial variability of nitrate and oxygen in Monterey Bay, California. The Dorado conducts missions up to 100 km in length. A very simplified diffusion and reaction model for nitrate, ignoring horizontal processes and advection and assuming steady state, would require that consumption rate = $K_Z \times \partial^2 NO_3^- / \partial Z^2$ (K_Z = vertical eddy diffusion coefficient). Water column regions exhibiting elevated nitrate uptake rates are identified from anomalies in the second derivatives of the vertical concentration profiles relative to the second derivative of conservative properties. The relationship between chlorophyll *a* fluorescence and the inferred productivity rates exhibits coherent spatial variability across the bay.

Patchiness in plankton distributions is a characteristic feature of the upper ocean (Martin 2003, 2005). The role of nutrients in regulating patchy distributions remains poorly understood. Moored nutrient sensors have only recently reached a state such that they can generate time series data that provide useful information on ecosystem processes (McGillicuddy et al. 1998; Sakamoto et al. 2004; Johnson et al. 2006). The ability to make high-spatial-resolution measurements of nutrient distributions in both horizontal and vertical dimensions within the ocean could provide important insights into the interaction of phytoplankton and their environment. However, mapping nutrient distributions at the same scales at which chlorophyll fluorescence intensity can be measured has been a challenge (Martin 2003). Underway mapping of surface nutrient distributions is feasible using shipboard chemical analyzers (Sakamoto et al. 1998; Woodward and Rees 2001). Relatively few such studies have been made that incorporate vertical resolution because of the difficulty in pumping water from depth while ships are underway. Specialized pumping systems are required in this case to deliver seawater to shipboard laboratories. Hales and Takahashi (2004) reported on an extensive set of nutrient and inorganic carbon measurements using a SeaSoar system with an integral pump to deliver water to the ship. Hales et al. (2005) demonstrated measurements with vertical resolution in nutrient measurements of several meters using submersible pumps towed behind a slowly moving ship to supply high-speed, automated chemical analyzers (Hales et al. 2004) operated in shipboard laboratories. The results reported by Hales et al. (2005) clearly demonstrate the novel and important insights that can be obtained with high-resolution nutrient measurements. However, such work can be quite labor-intensive, with personnel required to operate the ship, the pumping system and the laboratory analyzers.

Propeller-driven autonomous underwater vehicles (AUVs) are capable of making high-resolution surveys of ocean properties in relatively short times. These capabilities have been combined with physical sensors to study turbulence (Goodman et al. 2006) and with bio-optical sensors to study distributions of organisms (Brown et al. 2004; Moline et al. 2005). AUVs with similar sensors have also been used to study the coupling between ocean physics and biology (Yu et al. 2002; Ryan et al. 2005). Statham et al. (2005) have extended the sensor suite utilized on AUVs to include a reagent-based chemical analyzer that was used to measure dissolved manganese in a fjord. It is now feasible to include optical nutrient sensors (Johnson and Coletti 2002) in the suite of sensors mounted on AUVs. Such systems can greatly reduce the number of personnel required for repeated high-resolution chemical measurements. In this paper, the focus is on analyzing a set of nitrate and dissolved oxygen measurements made from the Monterey Bay Aquarium Research Institute (MBARI) Dorado AUV. We present data from a series of repeated occupations of a (primarily) north-to-south transect across Monterey Bay. A special emphasis is placed on exploring the feasibility of deriving phytoplankton metabolic rates

[1] Present address: OGI School of Science and Engineering, Oregon Health and Science University, 20000 NW Walker Road, Beaverton, Oregon 97006.

Acknowledgments

We thank the Dorado operations group, in particular Hans Thomas, and the crew of the RV *Zephyr* for supporting routine autonomous underwater vehicle missions. Carole Sakamoto and Luke Coletti supported operation and calibration of the in situ ultraviolet spectrophotometer nitrate sensor. We thank John Ryan and Todd Martz, who reviewed early drafts of the manuscript, as well as two anonymous reviewers.

This work was supported by the Monterey Bay Aquarium Research Institute through a grant from the David and Lucile Packard Foundation.

along this transect using small-scale spatial variability detected with chemical sensors.

Methods

The measurements reported here were made with a Dorado AUV (Sibenac et al. 2002) constructed at MBARI. The Dorado is a 53-cm-diameter, 3.9-m-length platform. It can make up to 100-km-length transects while undulating to a depth of 500 m and traveling at 5.5 km h^{-1} (1.5 m s^{-1}). The Dorado is equipped with a sensor suite that includes dual Sea-Bird conductivity and temperature sensors, an in situ ultraviolet spectrophotometer (ISUS) nitrate sensor (Johnson and Coletti 2002), a Sea-Bird 43 oxygen sensor, and a HobiLabs HS2, which is a chlorophyll *a* fluorometer and dual channel backscatter sensor for particle abundance (Sibenac et al. 2002). The sensors, with the exception of the HS2, are placed in a continuously pumped sample stream. The HS2 is flush-mounted in the hull and observes water flowing past the AUV. Chlorophyll fluorescence is reported here in the native units of the HS2, which reach maximum values during these transects of ~0.03 on an arbitrary scale. An approximate conversion of these arbitrary units to chlorophyll concentration (μg L^{-1}) is HS2 value/0.0007, which makes the largest chlorophyll fluorescence values approximately equivalent to 40 μg chlorophyll L^{-1}. When undulating to 100-m depth, the typical horizontal distance required for a complete down and up cycle is about 800 m. The Dorado surfaces to obtain a global positioning system fix at approximately 4-km intervals and navigation is interpolated between fixes using known speed and direction. The Dorado is operated in a completely unattended mode, with the vehicle released by its tender in late afternoon and retrieved at the end of its mission the following morning.

The ISUS nitrate sensor was operated at 0.7 Hz on these missions. Data from the other sensors were logged at a higher frequency of 4 Hz. At the end of each mission, a series of scripts download the data and produce a merged data file in the Ocean Data View (ODV; Schlitzer 2007) format with all sensor data decimated to the frequency of the ISUS nitrate data. This file contains about 17,000 observations for each mission discussed here. In addition, a Matlab mat file is produced with the complete data set for each sensor. All of the analyses performed here are based on the ODV file with all sensor data at a common sampling frequency. The scripts apply a constant lag term for each sensor in the pumped sample stream that was based on an estimate of the plumbed volume to each sensor and the seawater flow rate. Because of changes in plumbing of the system and pump speed, this lag correction was not completely accurate. An additional lag correction was applied for each sensor by examining offsets between data collected on up and down profiles on each mission.

The ISUS sensor calculates nitrate concentration using the algorithm described in Johnson and Coletti (2002). We have recently developed a revised algorithm that substantially improves the accuracy of ultraviolet (UV) nitrate measurements (C. Sakamoto et al. unpubl.). All of the data reported here were reprocessed with that new algorithm. This involves correcting the bromide molar absorptivities, which dominates the sea salt spectrum, to the in situ temperature. Although the nitrate spectrum is insensitive to temperature, the bromide spectrum is quite temperature-sensitive. This occurs because the bromide absorption band in the deep UV (<230 nm) results from a charge transfer to solvent complex (Jortner et al. 1964) and the interaction with solvent is temperature-dependent. In the revised algorithm, the salinity and temperature measured with the conductivity-temperature-depth (CTD) sensor are used to predict the in situ bromide spectrum using the well-known bromide to chlorinity ratio (Morris and Riley 1966) and bromide molar absorptivities measured as a function of temperature in the laboratory (C. Sakamoto et al. unpubl.). This bromide spectrum is then subtracted from the observed UV spectrum. Nitrate is determined by fitting the bromide-corrected seawater spectra with the molar absorptivities of nitrate, which are temperature-independent, and an absorbance baseline that is a linear function of wavelength. These recomputed nitrate concentrations are then substituted into the merged ODV file. The accuracy of nitrate concentrations calculated with the revised algorithm is significantly improved relative to the original algorithm, as shown by an extensive set of comparisons between sensor data and nitrate measurements made in the laboratory (C. Sakamoto et al. unpubl.). In relatively clear water, such as that found in Monterey Bay, and with little fouling of the sensor, which is achieved in the AUV by rinsing the optics before each mission, concentrations computed with the revised algorithm should be accurate to <1 μmol L^{-1} nitrate.

Results and discussion

Our focus in this paper is on repeated transects of 44-km length made across Monterey Bay by the Dorado AUV. These transects begin in water depths of approximately 15 m at the northern side of the bay and end in water depths near 50 m to the south (Fig. 1). The transects pass near the M1 mooring at the mouth of the bay, which is also equipped with an ISUS nitrate sensor at the surface (Johnson et al. 2006). During upwelling events, the M1 mooring is in the path of an upwelled plume of water that originates near Point Año Nuevo, to the north of Monterey Bay (Breaker and Broenkow 1994; Rosenfeld et al. 1994; Fitzwater et al. 2003). The water at the northern end of the transect lies in a feature that has been termed an upwelling shadow (Graham and Largier 1997). Water in the upwelling shadow often has higher chlorophyll concentrations than does the remainder of the bay (Ryan et al. 2008).

AUV transects are nominally made at 4-week intervals each year, although this schedule is often altered to accommodate process-oriented studies. Here we focus on a comparison of two seasonal periods consisting of four transects during June and July of 2005 (day of the year [YD] 161, 175, 182, and 203) and two transects in October and December of 2005 (YD 301 and 350). The June to July transects were selected because the mission was repeated at slightly greater than normal frequency, and the October and December transects were selected to represent a lower

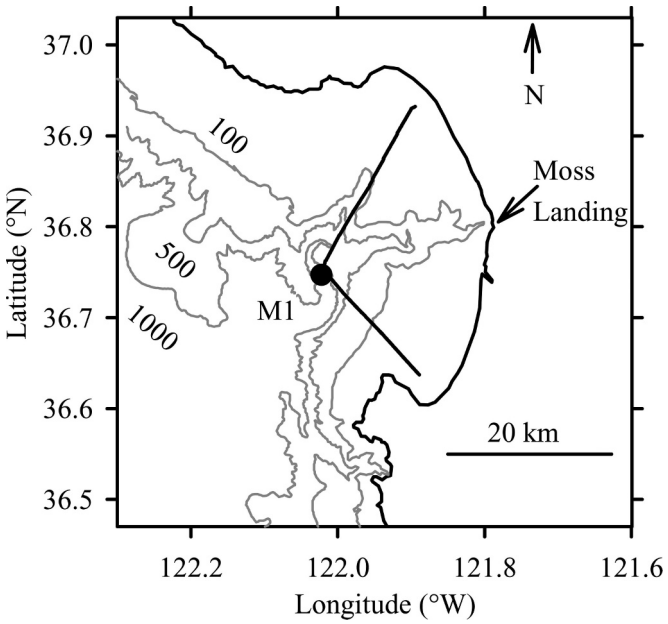

Fig. 1. Location of the AUV transect in Monterey Bay, California (solid line) and the M1 mooring (closed circle). Depth contours are 100 m, 500 m, and 1000 m.

productivity period in the same year. The June/July transects began during a period of relatively strong upwelling that slowly weakened (Fig. 2). The October to December period was characterized by weak upwelling or downwelling (Fig. 2). Each transect began near local sunset (04:00 h GMT, 21:00 h PDT in June and July and 01:00 h GMT, 17:00 h PST in October and December), and ended 8 h later, before sunrise. The diel amplitude of chlorophyll fluorescence quenching, which affects fluorometer-based measurements of chlorophyll during daylight (Falkowski and Kolber, 1995), is largely avoided by this timing.

Nitrate measurements from four of the transects (YD 161, 203, 301, and 350; corresponding calendar days are 10 June 2005, 22 July 2005, 28 October 2005, and 16 December 2005) are plotted vs. temperature and salinity in Fig. 3. The deep nitrate concentrations (typically >20 μmol L^{-1}) have a consistent relationship with both temperature and salinity over the 6-month period, which implies the persistence of a relatively constant deep-water end-member in the bay. However, in waters nearer to the surface, the nitrate concentrations have larger variability at constant temperature or salinity. Nitrate concentrations vary by about 10 μmol L^{-1} in waters at 12°C and by as much as 20 μmol L^{-1} in waters with a uniform salinity. As we discuss below, these differences appear to be driven primarily by changes in the rates of biologically driven nitrate utilization, as well as by local heating and cooling of surface waters.

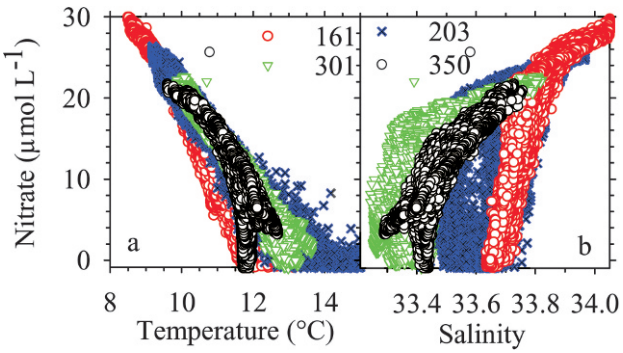

Fig. 3. Nitrate concentration plotted vs. (a) temperature and (b) salinity for AUV missions on YD 161, 203, 301, and 350 in 2005.

Distributions along transect

The distributions of temperature, salinity, nitrate, and chlorophyll fluorescence observed along the cross-bay transect are shown in Figs. 4–7 for YD 161, 203, 301, and 350. During the relatively strong upwelling conditions

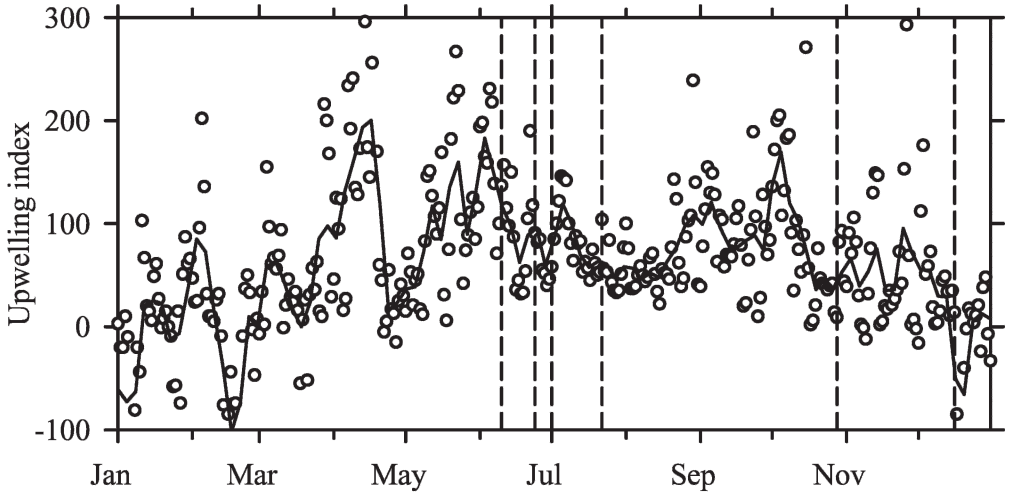

Fig. 2. Upwelling index (m^3 upwelled s^{-1} [100 m]$^{-1}$ coastline) at 36°N, 122°W, calculated from wind speed and direction. Daily values are shown as open circles, and the solid line is a 5-d running mean. Vertical dashed lines show times of the six AUV transects. Upwelling index values were downloaded from http://www.pfeg.noaa.gov.

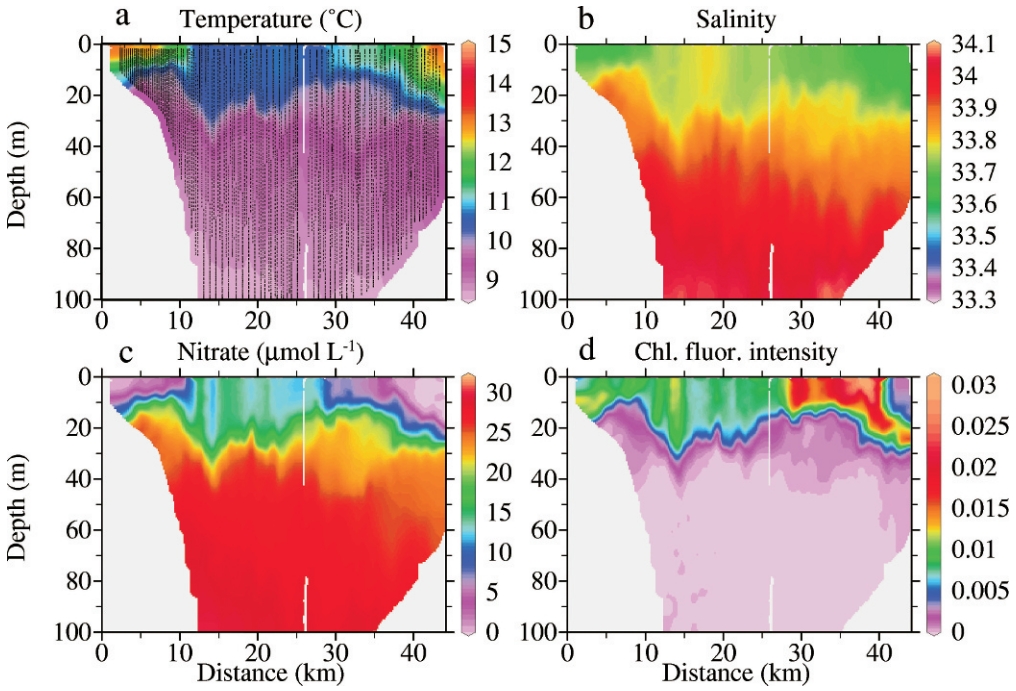

Fig. 4. (a) Temperature, (b) salinity, (c) nitrate, and (d) chlorophyll fluorescence intensity vs. depth and distance along the AUV transect on YD 161. Each measurement location is shown as a black dot on the temperature panel. These dots form a series of sawtoothed lines that track the AUV undulations. Distance is the elapsed distance from the northern end of the transect.

on YD 161 (Fig. 4), the surface water near the M1 mooring is cold (10.5°C) and it has high nitrate concentrations (highest values of 14 μmol L^{-1} at 20 km near M1) and a mean over the entire transect of 5.9 μmol L^{-1} in the upper 5 m. The high concentrations near M1 reflect the presence of the upwelling plume that originates near Point Año Nuevo (Rosenfeld et al. 1994; Fitzwater et al. 2003; Chase et al. 2005). The northern and southern ends of the transect are warmer, are nitrate-depleted, and have higher chlorophyll fluorescence intensity. Highest chlorophyll fluorescence is generally present near the surface in a 10–20-m-thick layer on this transect. A subsurface chlorophyll

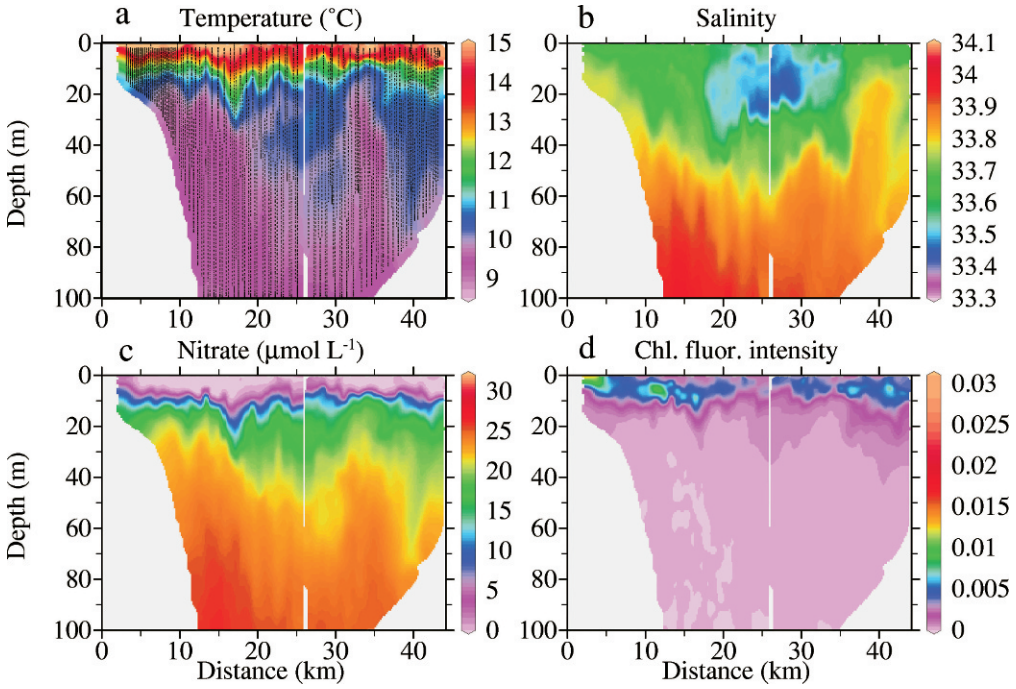

Fig. 5. As in Fig. 4 for the AUV transect on YD 203.

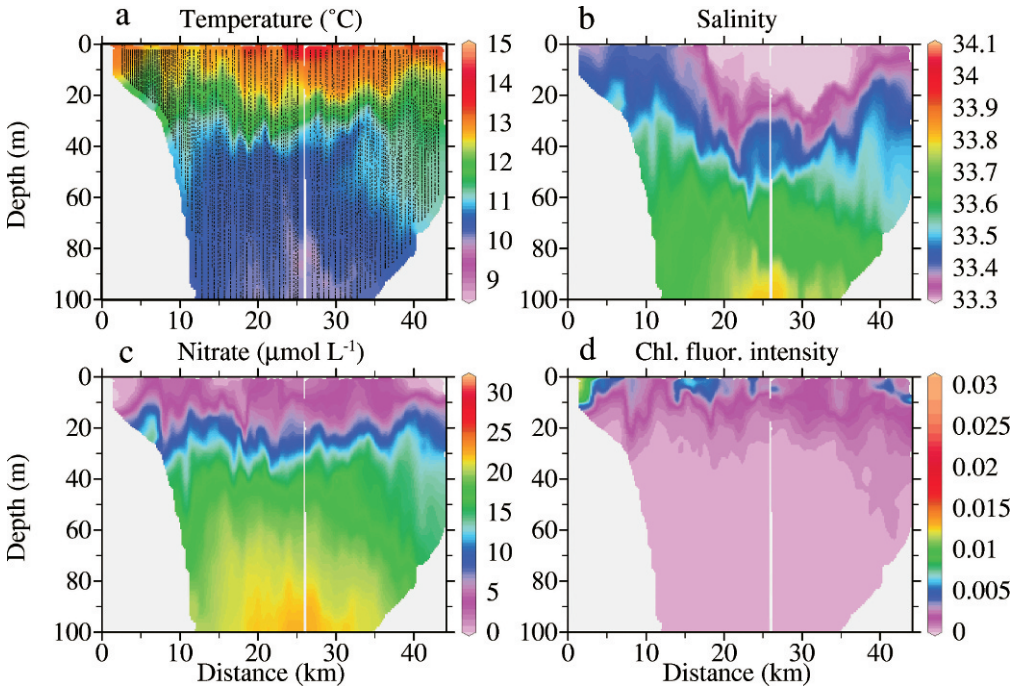

Fig. 6. As in Fig. 4 for the AUV transect on YD 301.

fluorescence intensity maximum was not found. By YD 203 (Fig. 5), upwelling intensity has diminished considerably and nitrate concentrations in surface waters are near zero across the entire transect (mean value of 0.12 μmol L^{-1} in the upper 5 m). Chlorophyll fluorescence intensities are lower and form a subsurface maximum near the nitracline, which was identified visually as the sharp gradient in nitrate concentration. The standard deviation for the <5-m nitrate data is 1.4 μmol L^{-1} on the YD 203 transect and, with n = 1690, the 95% confidence interval (CI) is 0.06 μmol L^{-1}. However, uncertainty in the calibration of the ISUS and in the spectral deconvolution algorithm add an additional, systematic uncertainty of 0.5 to 1 μmol L^{-1} that would occur as an absolute offset in all of the data for a given transect (C. Sakamoto et al. unpubl.). One should not consider the results more accurate than 1 μmol L^{-1} without

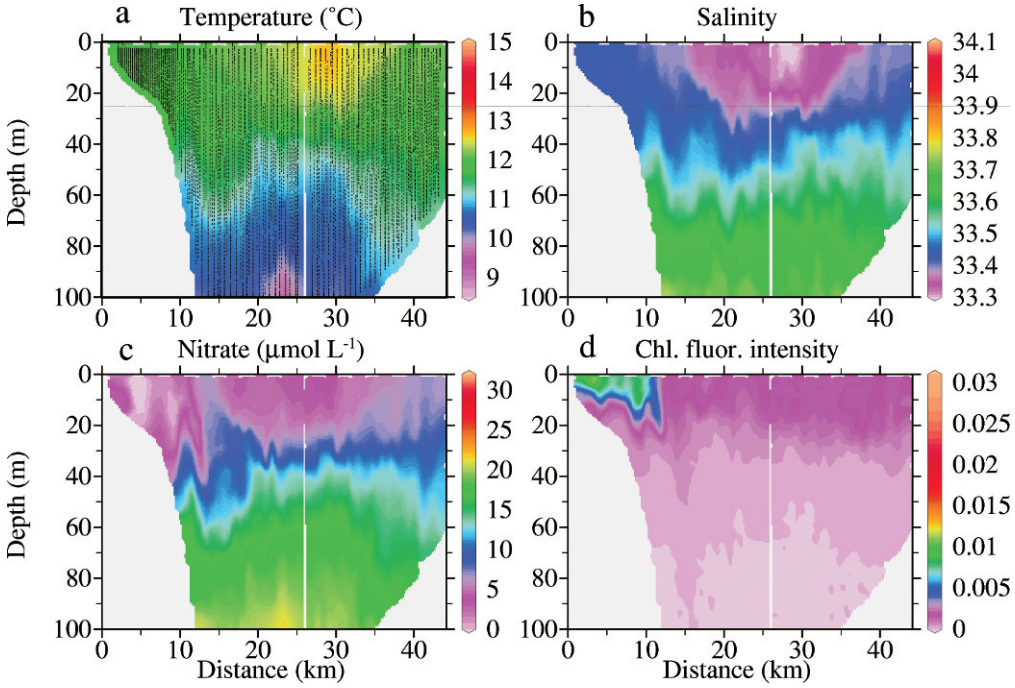

Fig. 7. As in Fig. 4 for the AUV transect on YD 350.

simultaneous laboratory measurements of nitrate to calibrate these potential systematic uncertainties. During late autumn, nitrate is relatively low in surface waters, but not completely depleted. Nitrate concentrations in the upper 5 m average 2.0 μmol L^{-1} on YD 301 (Fig. 6) and 3.1 μmol L^{-1} on YD 350 (Fig. 7). If there are systematic offsets in these concentrations, they will be towards higher concentrations, because there are coherent patches along each transect with zero nitrate concentrations. A negative offset would not be possible. We therefore consider these values to likely be higher than the YD 203 concentrations, particularly on YD 350. Despite the modest amounts of nitrate, there is little chlorophyll fluorescence detected on either transect, and the chlorophyll fluorescence maximum is near the surface and not in a subsurface maximum at the nitracline as on YD 203.

It is clear that there is an abundance of descriptive data that are obtained from the spatial and temporal variability that is detected along the cross-bay transect with in situ sensors. However, the capability of the AUV and chemical sensor combination to perform repeat missions with a relatively low overhead in terms of technical support would rapidly outstrip our capability for descriptive analyses of the information. For example, the Dorado AUV has completed more than 150 missions since 2003. The six transects described here represent <4% of the available data. Our primary interest, therefore, is in exploring the potential for using the biogeochemical data to obtain more quantitative metrics of ecosystem processes and metrics that can be produced as a standard product. One possible metric might be measurement of the abundance of dissolved nitrate. However, mean concentrations of nutrient chemicals such as nitrate are not a direct indicator of ecosystem processes, as can be seen by the very low chlorophyll fluorescence intensities on YD 301 and 350, despite the presence of modest nitrate concentrations. This may occur because limitation of phytoplankton growth is created by low light availability during deep mixing (Kudela and Dugdale 2000), or by low concentrations of other micronutrients, such as iron (Bruland et al. 2001; Johnson et al. 2001; Chase et al. 2005), which we do not measure autonomously.

The influence of biological processes on nitrate concentration can be seen in the plots of nitrate vs. temperature or salinity for each of the four transects shown in Fig. 8. In these plots, each data point is colored in proportion to the chlorophyll fluorescence intensity that was measured at the same time as nitrate. Nitrate concentrations exhibit nearly linear relationships with temperature and salinity in the deep portions of each transect (Fig. 8). Nitrate behaves as an essentially conservative tracer at these depths. Nearer the surface, deviations in nitrate concentration from linearity with temperature or salinity occur. Highest chlorophyll fluorescence intensities are seen in the regions of the plots where the data appear to deviate most strongly below a linear relationship. If we presume that the deeper, linear trends with temperature and salinity can be extrapolated towards the surface, the deviations indicate uptake of nitrate as the phytoplankton biomass increases. The relationship of nitrate with temperature appears to be complicated by the

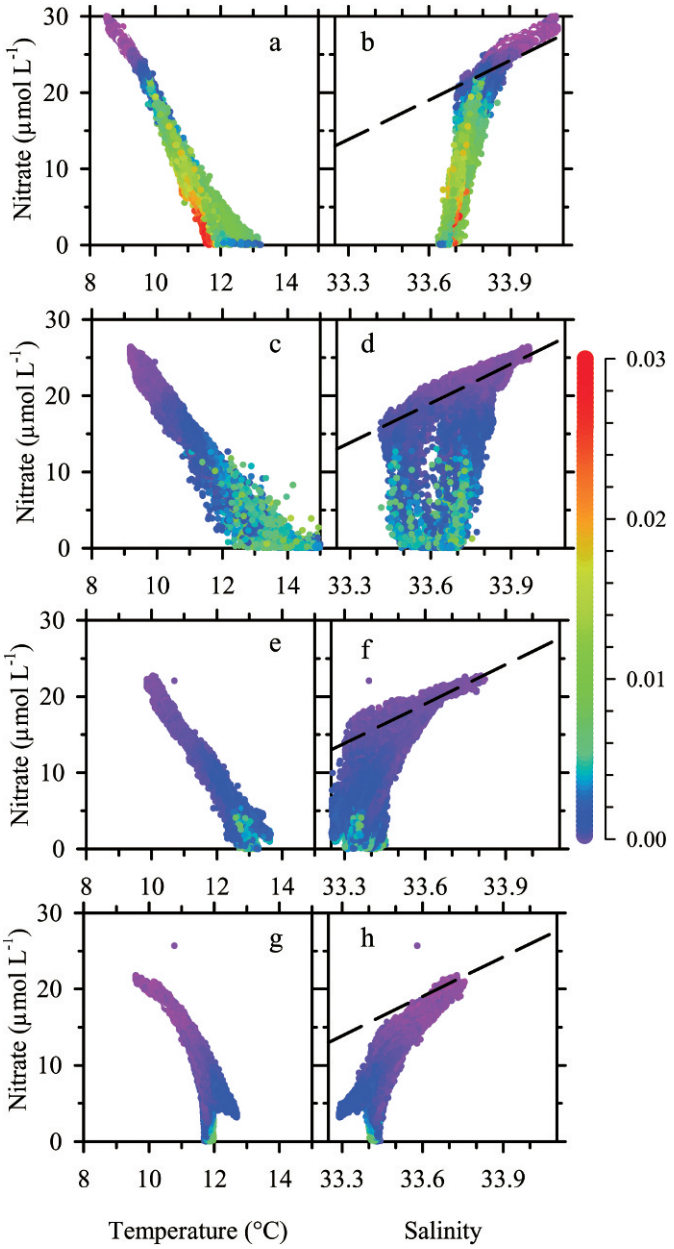

Fig. 8. Concentrations of nitrate are plotted vs. temperature and salinity for YD (a, b) 161, (c, d) 203, (e, f) 301, and (g, h) 350. Each data point is colored by the chlorophyll fluorescence intensity that was measured simultaneously. The solid line is the least squares line $NO_3^- = 12.989 + 17.236 \times (S - 33.25)$, which was fitted to deep samples.

effects of local heating and cooling, as well as nitrate uptake. This is illustrated by data for YD 350 (Fig. 8g), where the nitrate and temperature data show concave downward curvature. Air temperature preceding this AUV transect had been exceptionally cold, with nighttime lows near 0°C for many of the 10 d prior to the transect. The concave pattern appears to be because of surface cooling. On the other hand, local heating creates warm, low-nutrient surface water on many days (e.g., Fig. 8c). For this reason, we focus primarily on the nitrate and salinity relationship to identify regions where biological activity affects nitrate distributions.

During the time frame of this study there are no significant local factors affecting salinity in surface waters, such as freshwater inputs caused by rainfall events or flow from surrounding rivers.

The nitrate and salinity plots show a consistent, linear relationship in deep water (Figs. 3, 8). The linear trend line extrapolates to a low-salinity (32.5), nitrate-depleted water mass that would be characteristic of the California Current surface waters (Collins et al. 2003). The high-salinity (34), high-nitrate (27 μmol L^{-1}) water is characteristic of the upwelling source water mass found in Monterey Bay (Pennington and Chavez 2000). The deep trend line observed on the AUV transects in Monterey Bay is a linear mixing curve between California Current waters, which are completely depleted in nitrate, and the upwelling source waters with higher salinity and high nitrate concentrations. Near-surface deviations from the linear relationship observed in deep water must be driven to a large extent by biological uptake, because the points that fall furthest from the trend line tend to have the highest chlorophyll fluorescence intensity on each transect (Fig. 8).

Metabolic rate estimates

If the majority of new production in surface waters is derived from the supply of nutrients from below the euphotic zone (Dugdale and Goering 1967), then high rates of primary productivity should occur in areas with the largest nutrient inputs from vertical eddy diffusion. A method to distinguish regions of high nutrient uptake is to examine the vertical concentration gradient for depths where large changes occur in the slope—the second derivative—of a shallowing nutrient profile. A simple diffusion and reaction model for nitrate can be derived from the tracer conservation equation (Sarmiento and Gruber 2006). The model, which ignores horizontal processes and vertical advection and presumes a steady state, would require that regions of high nitrate second derivative are areas of elevated nutrient removal:

$$\mathrm{NO_3^-}\ \text{consumption rate} = K_Z \times \partial^2 \mathrm{NO_3^-} / \partial Z^2 \qquad (1)$$

The vertical eddy diffusion coefficient K_Z is presumed to be constant. We can use the high vertical and horizontal resolution in the AUV data to identify areas of Monterey Bay with high nitrate consumption rates by mapping the second derivatives of the vertical concentration profiles. Similarly, for oxygen,

$$\mathrm{O_2}\ \text{production rate} = -K_Z \times \partial^2 \mathrm{O_2} / \partial Z^2 \qquad (2)$$

where a calculation of oxygen production requires a minus sign on the right-hand side of the equation.

We calculated second derivatives for each property (P) by fitting a quadratic equation in depth to seven data points centered on each data point (a running quadratic fit in the same manner as a running mean):

$$P = a + b \times Z + c \times Z^2 \qquad (3)$$

The second derivative is then $2 \times c$. More points were not used to calculate the second derivative because the quadratic is a relatively stiff equation that will not reproduce sharp changes in profiles when fitted over a broad depth range. As a result of the short fit window, these second derivatives are somewhat noisy, and a five-point running mean was used to further smooth the results. Also, the second derivative was not calculated if the depth range spanned by the seven points was less than 1.5 m, which frequently occurred near the top or bottom of an undulation as the AUV reduced its vertical velocity from typical rates near 0.5 m s^{-1}.

The Monterey Bay area is a region of strong coastal upwelling, and one might expect that vertical advection would dominate over vertical eddy diffusion. However, upwelling is localized to a few geographic areas (Rosenfeld et al. 1994; Chase et al. 2005) and the effects of upwelling through most of the bay are produced by lateral transport of the upwelled plume (e.g., Graham and Largier 1997). A scaling analysis of the expected importance of various transport mechanisms was made using observed gradients of properties and the expected values for horizontal and vertical velocities and horizontal (Okubo, 1971) and vertical (Carter and Gregg 2002; Kunze et al. 2002) eddy diffusion coefficients. This analysis (data not shown) suggests that vertical diffusion will dominate transport in areas away from centers of active upwelling, except when horizontal velocities are greater than about 0.1 m s^{-1}. Horizontal advection will then clearly dominate transport. Although short-term horizontal velocities approach 0.5 m s^{-1}, the average velocities over several days are typically much smaller (Graham and Largier 1997). It will require several days for phytoplankton processes to deplete nutrients at rates typical of Monterey Bay (Johnson et al. 2006). We therefore base our analysis on the premise that, because of the lower mean horizontal velocities over multiple days, vertical diffusion will dominate nitrate transport to the euphotic zone. Further, vertical distributions of biologically active chemicals such as nitrate and oxygen are anisotropic, with highest nitrate at depth and lowest values near the surface. Such resilient anisotropy is not present in horizontal distributions in most cases. Averaging over time or horizontal distance will tend to minimize horizontal gradients but not vertical gradients. This should again minimize the influence of horizontal transport.

The profiles of salinity, oxygen, nitrate, and temperature and their second derivatives are shown in Fig. 9 for vertical profiles by the AUV at 35 and at 5 km along the transect on YD 161. The second derivatives of salinity, oxygen, and nitrate in the upper 30 m are also contoured in Fig. 10 for the YD 161 transect. Several points are apparent in these plots. First, the second-derivative maximum for nitrate and minimum for oxygen are often displaced above the second-derivative maximum of salinity. This offset is apparent over most of the YD 161 transect, with the exception of the first 10 km in relatively shallow water (Fig. 10). The vertical profiles at 35 km (Fig. 9a–d) were selected to illustrate this behavior. The high second derivatives of nitrate and oxygen in this region of the transect are not simply produced by interleaving of water masses with different properties, an effect that Craig (1974) called "masquerading." If this were

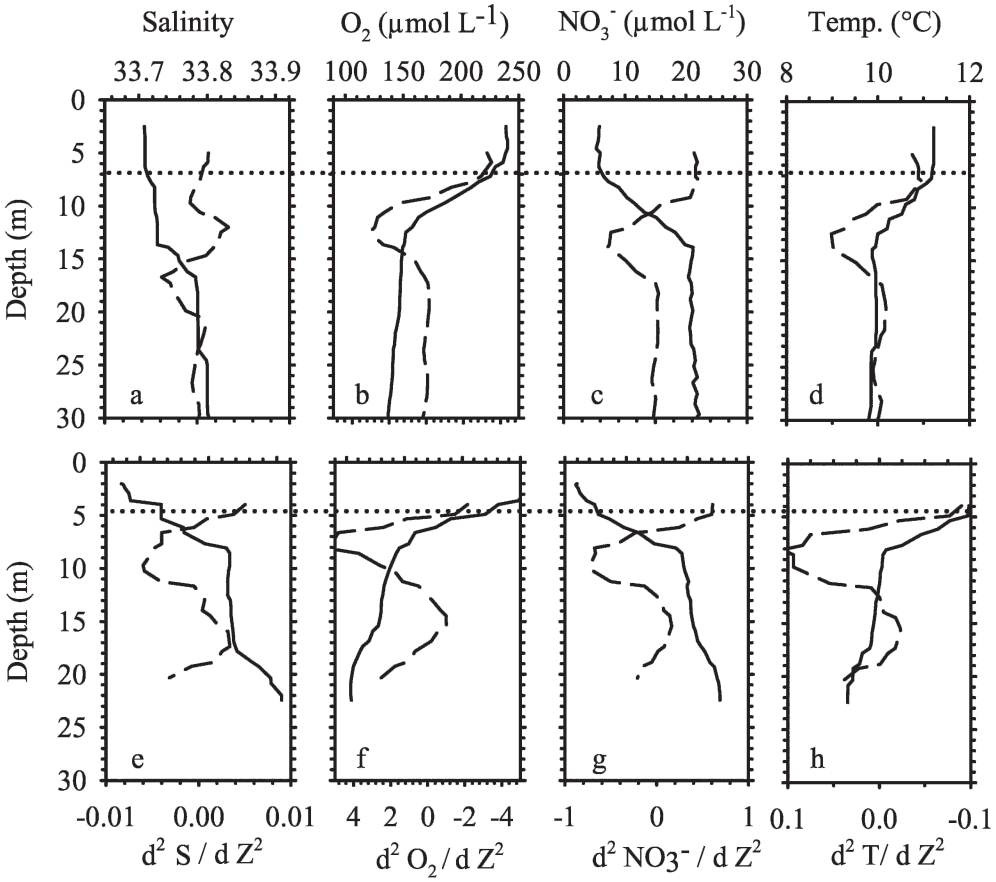

Fig. 9. Vertical profiles of (a) salinity, (b) oxygen, (c) nitrate, and (d) temperature at 35-km distance along the YD 161 transect are shown as solid lines. Second derivatives of each property are plotted as dotted lines. Vertical profiles at 5 km along the transect for (e) salinity, (f) oxygen, (g) nitrate, and (h) temperature and their second derivatives are also shown. Note that the scales for oxygen and temperature second derivatives are reversed so that values corresponding to oxygen production, nitrate consumption, and heat input all lie on the right-hand side of the axis. The horizontal line passes near the maximum second derivative of nitrate and the minimum values of the oxygen and temperature second derivatives.

the case, the extrema in second derivatives of all properties would be coincident. The second-derivative maximum for nitrate and minimum for oxygen must be produced by biogeochemical processes that alter chemical distributions, in addition to physical processes. In the first 10 km of the transect, however, the second derivatives of all four properties have coincident extrema (Figs. 9e–h, 10). In these shallow waters (<20 m), physical stirring of the water column appears to create interleaving and synchronized second derivatives. The distributions of chlorophyll fluorescence intensity along the transect support this interpretation. From 30 to 40 km, the large positive second derivatives of nitrate and negative second derivatives of oxygen are not mirrored by corresponding salinity second derivatives (Fig. 10). This is, however, the region of largest chlorophyll fluorescence intensity, which is indicative of highest biomass and oxygen production and consumption of nitrate. In the inner 10 km of the transect, the chlorophyll fluorescence intensity is low and there does not appear to be sufficient biomass to support large amounts of nitrate consumption or oxygen production (Fig. 10). Physical stirring must dominate.

The second derivative of temperature does have extrema coincident with those of nitrate and oxygen (Fig. 9). The close correlation between structure in temperature and biogeochemical properties must result from the input of solar energy that simultaneously drives local heating and photosynthesis. Nitrate and temperature values measured on the M1 mooring during the week of the YD 161 transect are shown in Fig. 11. As nitrate is drawn down each day by phytoplankton uptake (Johnson et al. 2006), temperature increases near the surface because of local heating. Nitrate concentration changes have a much weaker correlation with salinity; often there is no correlation with salinity (Fig. 11d). This confirms that the linked changes in temperature and nitrate are a result of local heating and primary production, rather than water mass changes. Because of the confounding influence of local heating on temperature, we focus on salinity as a tracer of mixing processes.

It is clear from the mooring nitrate data in Fig. 11 that there is a strong diel cycle in chemical properties driven by biogeochemical processes during the time of the AUV surveys, as noted previously (Johnson et al. 2006). The

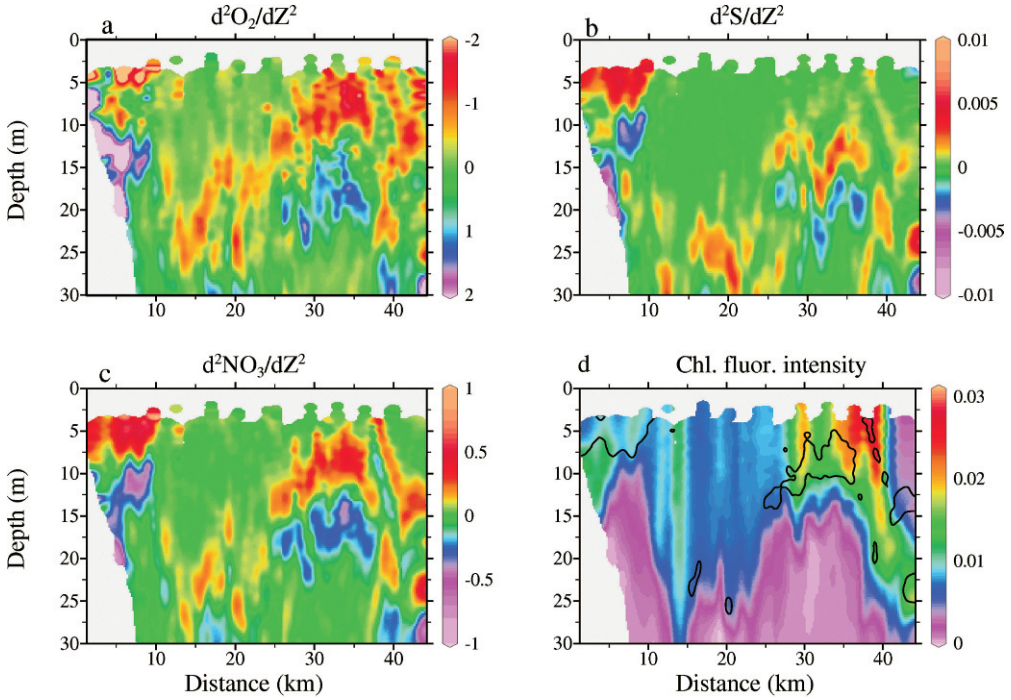

Fig. 10. Contoured sections of the second derivatives of (a) oxygen, (b) salinity, and (c) nitrate are shown with (d) the contoured section of chlorophyll fluorescence intensity for the AUV transect on YD 161. Solid contour lines overlain on chlorophyll fluorescence intensity (d) correspond to nitrate second derivative values of 0.2 mmol m^{-5}.

assumption of a steady state in Eqs. 1 and 2 must introduce some error. However, we proceed with this assumption for the following reason. The distributions of nitrate and oxygen and their second derivatives were always measured at night and reflect the period in the diel cycle where photosynthesis is expected to be low or zero. The changes in nitrate and oxygen between each 24-h nighttime period are much smaller than the photoperiod fluctuations (Fig. 11), and most likely reflect the magnitude of net nitrate utilization in the entire euphotic zone and not just the near surface. The changes in variables at this time scale occur over several day periods. Presumably, the biases in estimating metabolic rates from a steady-state model are reduced because of the timing of the sample period. As mentioned above, the influences of horizontal transport are also likely to be reduced when averaged over several days.

Calculation of the biogeochemical rates requires knowledge of the vertical eddy diffusion coefficient. Hales et al. (2005) used coincident measurements of K_Z and vertical nutrient distributions to calculate instantaneous chemical fluxes from the first derivatives. It is also feasible to measure instantaneous values of K_Z with sensors deployed on an AUV (Goodman et al. 2006), but the Dorado vehicle is not similarly equipped. The eddy diffusion coefficient can be estimated from the equation (Osborn 1980)

$$K_Z < 0.2\varepsilon/N^2 \tag{4}$$

where ε is the turbulence energy dissipation rate and N is the Brunt-Vaisala frequency. N can be calculated from the density gradient and ε could be estimated from current shear detected with the AUV's digital velocity log (Fong and Jones 2006). However, directly measured K_Z values and values estimated from Eq. 4 vary by three orders of magnitude in the upper water column (e.g., Carter and Gregg 2002; Kunze et al. 2002; Hales et al. 2005). If metabolic rates were estimated using such K_Z values, they would have unrealistic high variability because of the high frequency fluctuations in K_Z. The chemical distributions in the water column that produce the second derivatives must reflect the effects of phytoplankton processes over time scales on the order of several days given rates at which phytoplankton consume nutrients (Johnson et al. 2006). A calculation of metabolic rates from chemical distributions should use a value of K_Z that is scaled over the same time frame required for metabolic processes to structure chemical properties.

An extensive set of measurements of K_Z in Monterey Bay has been made in several studies (Carter and Gregg 2002; Kunze et al. 2002; L. Goodman pers. comm.). Observed values range over three orders of magnitude and reach 10^{-2} m^2 s^{-1}, particularly over the Monterey Canyon, where diapycnal mixing is extremely high. Based on the values of K_Z in the upper 100 m of Monterey Bay that were observed in each of these studies, we have adopted a value of 3×10^{-4} m^2 s^{-1}. This value implies that the root mean square time for vertical eddy diffusion to transport chemicals over a distance of 5 m, which is a characteristic vertical distance scale for structure in the second derivatives (Fig. 10), is $Z^2/(2 \times K_Z) = 0.5$ d (Mann and Lazier 2006). This calculation indicates that vertical eddy diffusion coefficients need to be averaged over time scales of

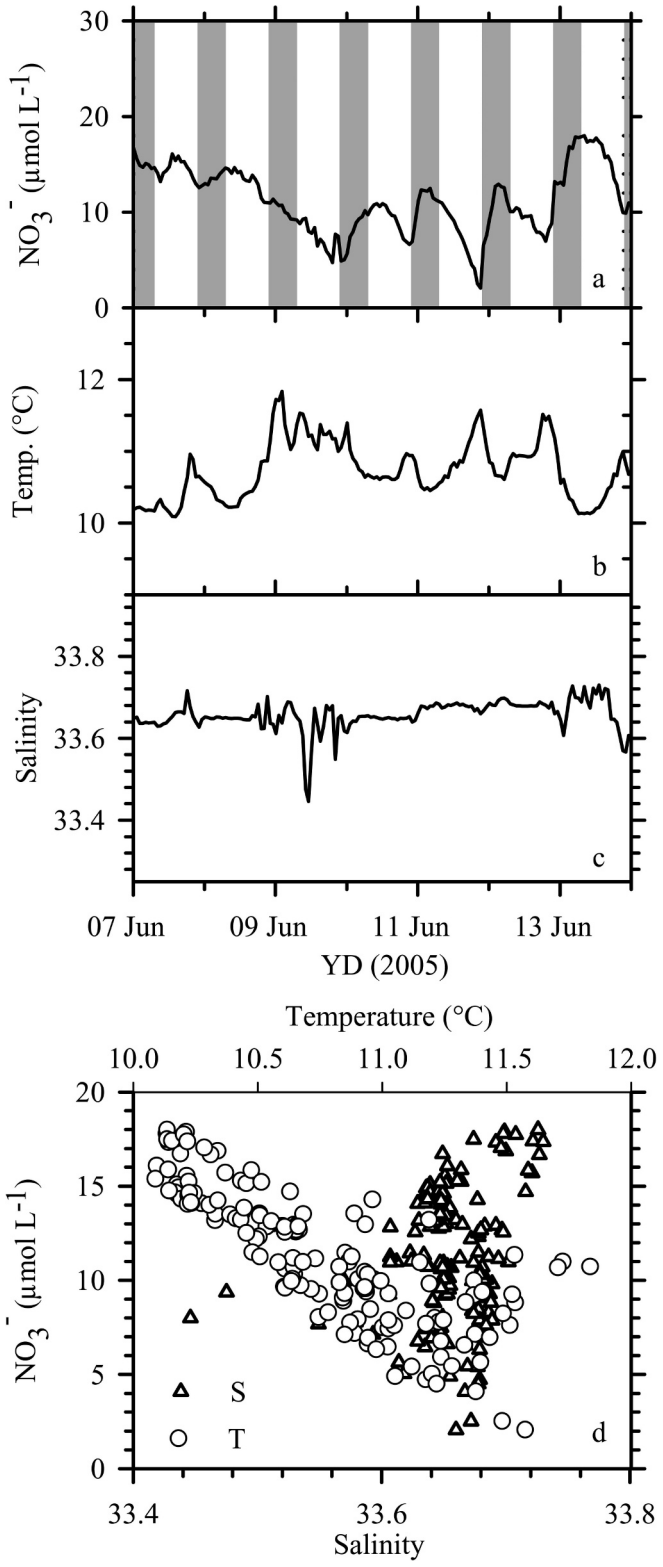

Fig. 11. (a) Nitrate, (b) temperature, and (c) salinity measured at 1 m depth on the M1 mooring over 1 week in June 2005. Grey bars (a) show dark period. (d) Nitrate plotted vs. salinity (triangles) and temperature (circles).

approximately 1 d to represent the net effects of diffusive transport, and it supports our choice of using a constant eddy diffusion coefficient.

The rates of nitrate consumption from Eq. 1 and oxygen production from Eq. 2 were both converted to units of carbon production (mg C m^{-3} d^{-1}) using the Redfield C:NO_3^- ratio of 106/16 and a modified Redfield C : O_2 ratio of 106 : 150 (Anderson 1995). Contour plots of the carbon production rates derived from second derivatives of nitrate and oxygen for the YD 161 AUV transect are shown along with contoured sections of chlorophyll fluorescence intensity in Fig. 12. The estimates of carbon production derived from the second derivatives of nitrate and oxygen show similar distributions along the section. A model II regression (Laws 1997) of the carbon production rates derived from nitrate vs. those derived from oxygen has a slope of 1.38 ± 0.02 (95% CI, $r = 0.63$). The nitrate-based estimate is likely slightly higher than the oxygen-based estimate because losses of dissolved O_2 by equilibration with the atmosphere will reduce the productivity signature.

Superimposed on the contoured plot of chlorophyll fluorescence intensity is the 250 mg C m^{-3} d^{-1} contour line for the rate derived from the nitrate second derivative (Fig. 12b). The regions with the highest apparent rates of carbon production are generally coincident with the areas of highest chlorophyll fluorescence intensity on the section, but there are also notable differences. For example, the nitrate second derivative (or apparent C production) values are high from 1 to 10 km along the transect, whereas chlorophyll fluorescence intensities are low. As we discussed above, this region also has large second derivatives of salinity, and the apparently large estimates of carbon production in the first 10 km are an artifact caused by physical interleaving of water with different properties. This general level of correspondence is similar for all six of the AUV transects. Given the large number of assumptions that are inherent in the estimate of metabolic rates, the moderate coincidence of the spatial distributions of the nitrate and oxygen second derivatives with that of chlorophyll fluorescence intensity is not surprising. There are other processes affecting the chemical distributions and phytoplankton biomass (e.g., grazing or export of biomass and vertical migration). However, a major factor altering the nitrate and oxygen distributions must be the linked biological uptake of nitrogen and production of oxygen as particulate organic matter is produced.

Averaging carbon production rates over multiple AUV missions should further minimize errors introduced by the assumptions that are inherent in Eqs. 1 and 2. For example, averaging should reduce biases introduced by assumptions of steady state and might also be expected to minimize the effects of horizontal processes, because frontal positions should move in response to changes in wind stress. We therefore averaged the second derivative of nitrate from the four June and July AUV transects and the two October to December transects and converted these means to carbon production rates. These mean rates are contoured along the cross-bay transect in Fig. 13 along with the mean section of chlorophyll fluorescence intensity for the summer and late fall time periods. The inferred rates

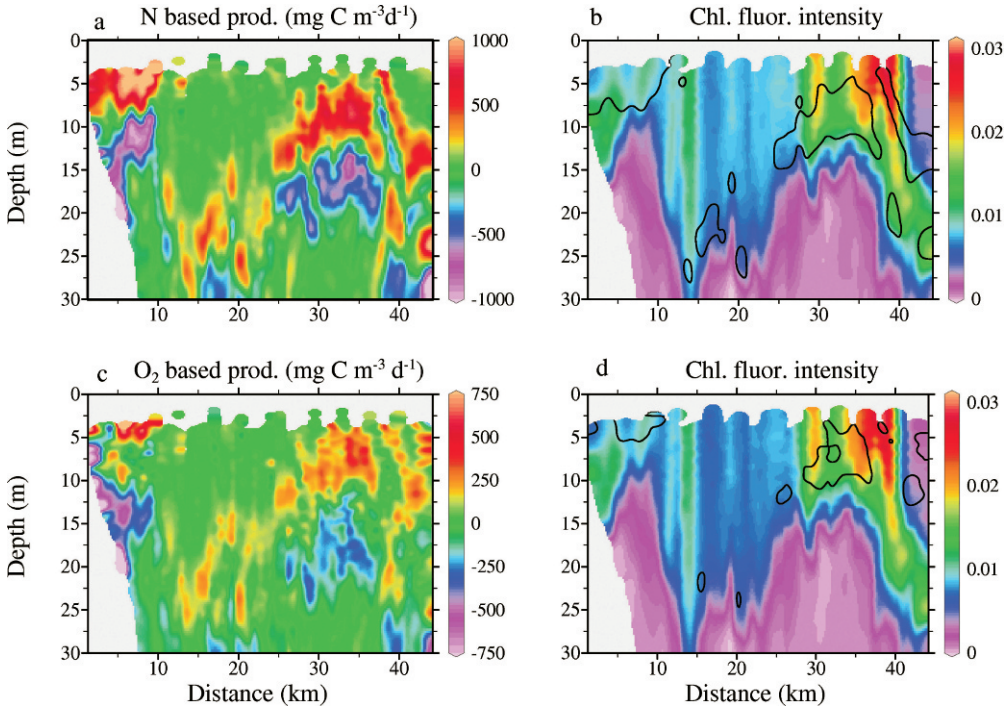

Fig. 12. Carbon production values derived from (a) nitrate and (b) oxygen second derivatives for the AUV transect on YD 161. The chlorophyll fluorescence intensity is shown (c, d). The contour line in (c) corresponds to the 250 mg C m^{-3} d^{-1} production value, derived from nitrate distributions. The contour line in (d) corresponds to the 200 mg C m^{-3} d^{-1} production value, derived from oxygen distributions.

of carbon production are substantially larger in the upper 10 m during June and July (223 ± 28 mg C m^{-3} d^{-1}, 95% CI) than in October and December (37 ± 12 mg C m^{-3} d^{-1}). These seasonal differences in metabolic rates determined from the AUV data reflect observed seasonal changes in the primary production of Monterey Bay averaged over 8 yr (Fig. 14; Pennington and Chavez 2000). The rates measured by the ^{14}C method and averaged over 8 yr decrease by a factor of 3.5 from summer to winter. Spatial variations in the inferred carbon production rates are also apparent, with highest rates in the shallow water at the northern and southern ends of the transect. Although we noted the artifacts in carbon production rates on YD 161 at the northern end of the transect, high mean rates on the inshore ends of the transect are in agreement with in situ and remote sensing observations that show persistent high chlorophyll in the inner parts of the bay (Graham and Largier 1997; Ryan et al. 2008).

The second derivative of nitrate in subsurface waters is negative, which indicates production of nitrate (Fig. 9c). This production could include both a flux of nitrate from deep waters and nitrification (e.g., Wankel et al. 2007) that, at steady state, supplies the nitrate consumed in the surface layer. Similarly for temperature, there is a negative second derivative near the surface indicating production of heat and a positive second derivative at depth, which is a sink for the heat (Fig. 9d). If our assumptions of approximate steady state and constant K_Z are correct, then the supply of nitrate from deep waters must balance consumption near the surface. Summer rates of nitrate supply (expressed as C supply using the Redfield ratio) and averaged from 10 to 60 m were −46 ± 6 mg C m^{-3} d^{-1}, and late fall rates were −2 ± 7 mg C m^{-3} d^{-1} (Fig. 13). These rates indicate an approximate balance between nitrate consumption (expressed as carbon production) (10 m × 223 = 2230 ± 280 mg C m^{-2} d^{-1}) and supply (50 m × −46 = −2300 ± 300 mg C m^{-2} d^{-1}) during summer. Fall rates of consumption (370 ± 120 mg C m^{-2} d^{-1}) and supply (−100 ± 350 mg C m^{-2} d^{-1}) are also similar. This comparison supports our assumptions of steady state and a constant value of K_Z when AUV data are averaged over multiple transects to obtain a view of spatial variability in rates.

The assumption of steady state appears to hold for individual days when apparent rates of C production are averaged over the entire AUV transect. The integrated rates of C production determined from the nitrate second derivative in the upper 10 m and in the depth range from 10 to 60 m are plotted vs. day of year in Fig. 14. On each of the six transects there is a near equivalence between the two integrals, indicating that rates of consumption and supply are in balance. Further, the rate of C production in the upper 10 m has a magnitude and temporal pattern that is generally similar to the multiyear (1989 to 1996) mean annual cycle of ^{14}C primary production (Pennington and Chavez, 2000) that has been measured at the M1 mooring site (Fig. 14). The agreement again suggests that the assumptions that we have made are reasonable when AUV data are averaged over a sufficiently large area for transects on a single day.

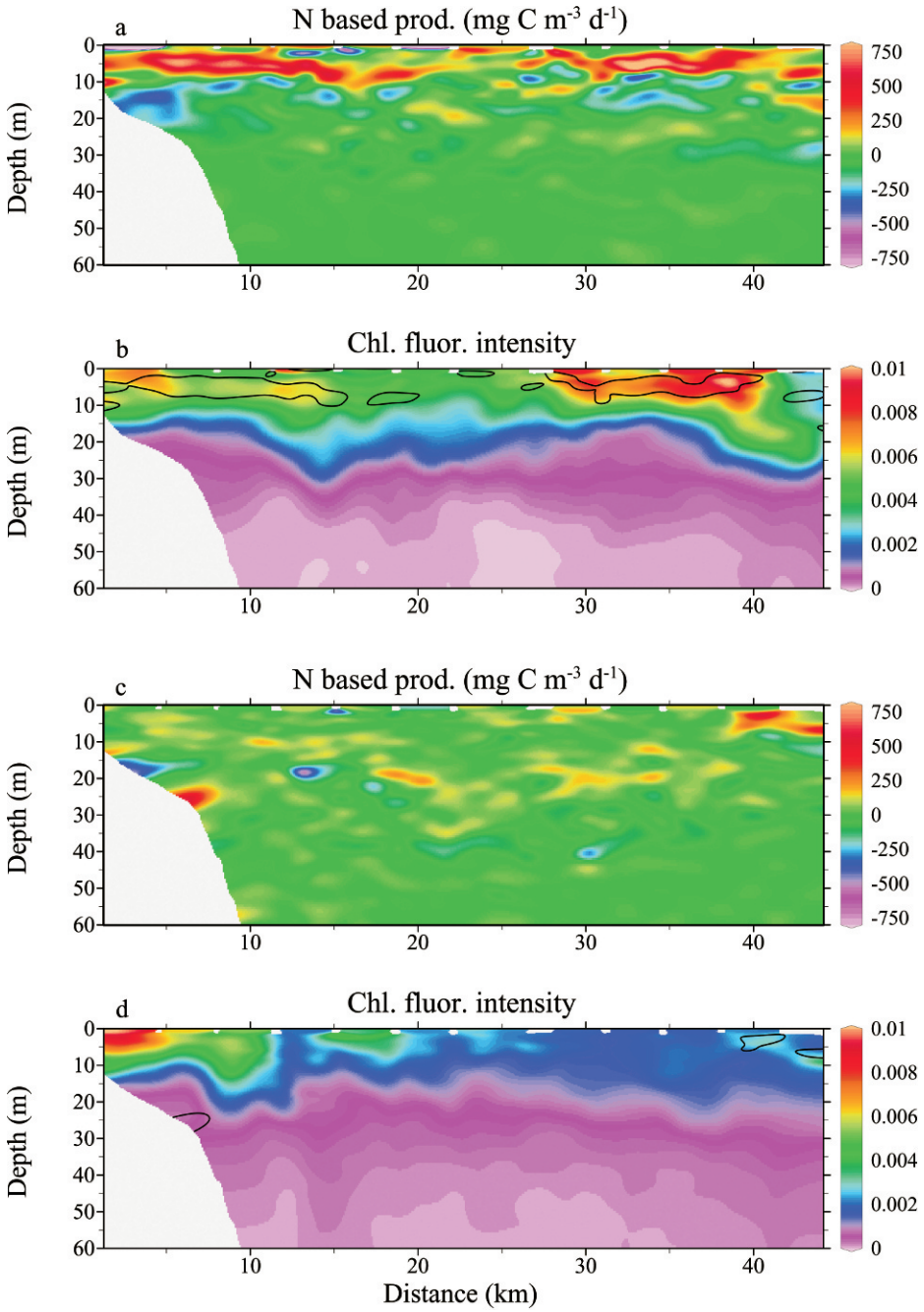

Fig. 13. Contoured sections of the mean carbon production estimated from the nitrate second derivative (A) and chlorophyll fluorescence intensity (B) for four AUV transects in June and July. Contoured sections of the mean carbon production estimated from the nitrate second derivative (C) and chlorophyll fluorescence intensity (D) for two AUV transects in October and December. The 250 mg C m^{-3} d^{-1} contour for C production is shown as a black line in (B) and (D).

Routine mapping of nitrate and oxygen concentration from autonomous vehicles is now feasible. These systems can generate impressively large data sets with relatively little effort once the sensors and platforms are integrated. By analogy to ocean color satellites, the challenge then is to develop quantitative products that can be routinely produced from the observations. The results presented here illustrate some of the potential to use AUVs equipped with chemical sensors to generate estimates of the spatial and temporal variability in plankton rate processes. The results also illustrate the issues that must be overcome to make these results truly quantitative. For example, calculation of rates is directly dependent on assumptions that we make about physical processes. The vertical eddy diffusion coefficient K_Z directly affects the rate calculations. Ultimately, the most effective use of tools such as

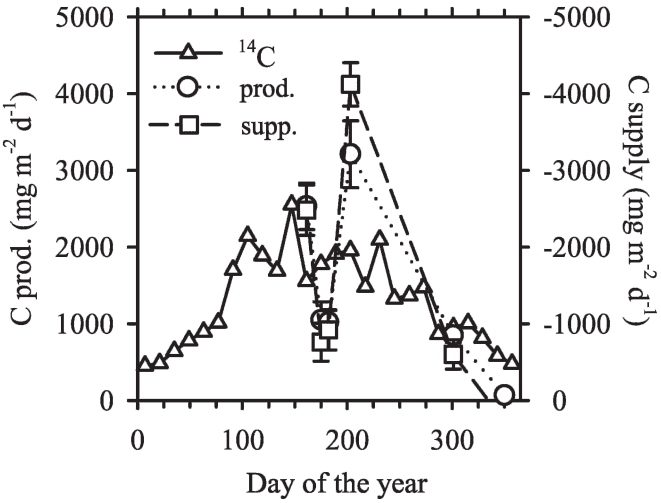

Fig. 14. Integrated C production values (mg C m^{-2} d^{-1}) in the upper 10 m of the water column, which were calculated from the nitrate second derivative and the Redfield C:NO_3^- ratio of 6.6 are shown as solid diamonds for each of the six AUV transects considered here. Integrated rates of nitrate resupply in the depth range from 10 to 50 m are shown, and also, converted to C units, are shown as solid squares. These values are plotted relative to the right-hand axis. The annual cycle of integrated primary production determined from 24-h incubations with ^{14}C at the M1 mooring site (Pennington and Chavez, 2000) that are averaged using 8 yr of data from 1989 to 1996 are shown as open triangles. ^{14}C data available at www.mbari.org/BOG.

AUV and chemical sensor combinations may be to incorporate their results into data-driven, inverse models (Schlitzer, 2002). Until such improved methods of data treatment are possible, the approach that we have used serves as a basis to examine variability in plankton rate processes.

References

Anderson, L. A. 1995. On the hydrogen and oxygen content of marine phytoplankton. Deep-Sea Res. I **42:** 1675–1680.

Breaker, L. C., and W. W. Broenkow. 1994. The circulation of Monterey Bay and related processes. Oceanogr. Mar. Biol. Annu. Rev. **32:** 1–64.

Brown, C. A., Y. Huot, M. J. Purcell, J. J. Cullen, and M. R. Lewis. 2004. Mapping coastal optical and biogeochemical variability using an autonomous underwater vehicle and a new bio-optical inversion algorithm. Limnol. Oceanogr. Methods **2:** 262–281.

Bruland, K. W., E. L. Rue, and G. J. Smith. 2001. Iron and macronutrients in California coastal upwelling regimes: Implications for diatom blooms. Limnol. Oceanogr. **46:** 1661–1674.

Carter, G. S., and M. C. Gregg. 2002. Intense, variable mixing near the head of Monterey Submarine Canyon. J. Phys. Oceanogr. **32:** 3145–3165.

Chase, Z., K. S. Johnson, V. A. Elrod, J. N. Plant, S. E. Fitzwater, L. Pickell, and C. M. Sakamoto. 2005. Manganese and iron distributions off central California influenced by upwelling and shelf width. Mar. Chem. **95:** 235–254.

Collins, C. A., J. T. Pennington, C. G. Castro, T. A. Rago, and F. P. Chavez. 2003. The California Current system off Monterey, California: Physical and biological coupling. Deep-Sea Res. II **50:** 2389–2404.

Craig, H. 1974. A scavenging model for trace elements in the deep sea. Earth Planet. Sci. Lett. **23:** 149–159.

Dugdale, R. C., and J. J. Goering. 1967. Uptake of new and regenerated forms of nitrogen in primary productivity. Limnol. Oceanogr. **12:** 196–207.

Falkowski, P. G., and Z. Kolber. 1995. Variations in chlorophyll fluorescence yields in phytoplankton in the world ocean. Aust. J. Plant Physiol. **22:** 341–345.

Fitzwater, S. E., and others. 2003. Iron, nutrient and phytoplankton biomass relationships in upwelled waters of the California coastal system. Cont. Shelf Res. **23:** 1523–1544.

Fong, D. A., and N. L. Jones. 2006. Evaluation of AUV-based ADCP measurements. Limnol. Oceanogr. Methods **4:** 58–67.

Goodman, L., E. R. Levine, and R. G. Lueck. 2006. On measuring the terms of the turbulent kinetic energy budget from an AUV. J. Atmos. Ocean. Technol. **23:** 977–990.

Graham, W. M., and J. L. Largier. 1997. Upwelling shadows as nearshore retention sites: The example of northern Monterey Bay. Cont. Shelf Res. **17:** 509–532.

Hales, B., J. N. Moum, P. Covert, and A. Perlin. 2005. Irreversible nitrate fluxes due to turbulent mixing in a coastal upwelling system. J. Geophys. Res. **110:** C10S11, doi:10.1029/2004JC002685.

———, and T. Takahashi. 2004. High-resolution biogeochemical investigation of the Ross Sea, Antarctica, during the AESOPS (U.S. JGOFS) Program. Glob. Biogeochem. Cycles **18:** GB3006, doi:10.1029/2003GB002165.

———, L. van Geen, and T. Takahashi. 2004. High-frequency measurement of seawater chemistry: Flow-injection analysis of macronutrients. Limnol. Oceanogr. Methods **2:** 91–101.

Johnson, K. S., F. P. Chavez, V. A. Elrod, S. E. Fitzwater, J. T. Pennington, K. R. Buck, and P. M. Walz. 2001. The annual cycle of iron and the biological response in central California coastal waters. Geophys. Res. Lett. **28:** 1247–1250.

———, and L. J. Coletti. 2002. In situ ultraviolet spectrophotometry for high resolution and long term monitoring of nitrate, bromide and bisulfide in the ocean. Deep-Sea Res. I **49:** 1291–1305.

———, ———, and F. P. Chavez. 2006. Diel nitrate cycles observed with in situ sensors predict monthly and annual new production. Deep-Sea Res. I **53:** 561–573.

Jortner, J., M. Ottolenghi, and G. Stein. 1964. On the photochemistry of aqueous solutions of chloride, bromide, and iodide ions. J. Phys. Chem. **68:** 247–255.

Kudela, R. M., and R. C. Dugdale. 2000. Nutrient regulation of phytoplankton productivity in Monterey Bay, California. Deep-Sea Res. II **47:** 1023–1053.

Kunze, E., L. K. Rosenfeld, G. S. Carter, and M. C. Gregg. 2002. Internal waves in Monterey Submarine Canyon. J. Phys. Oceanogr. **32:** 1890–1913.

Laws, E. A. 1997. Mathematical methods for oceanographers: An introduction. Wiley-Interscience.

Mann, K. H., and J. R. N. Lazier. 2006. Dynamics of marine ecosystems, 3rd ed. Blackwell.

Martin, A. 2005. The kaleidoscope ocean. Philos. Trans. R. Soc. Lond. A **363:** 2873–2890.

Martin, A. P. 2003. Phytoplankton patchiness: The role of lateral stirring and mixing. Prog. Oceanogr. **57:** 125–174.

McGillicuddy, D. J., Jr., and others. 1998. Influence of mesoscale eddies on new production in the Sargasso Sea. Nature **394:** 263–266.

Moline, M., and others. 2005. Remote Environmental Monitoring Units: An autonomous vehicle for characterizing coastal environments. J. Atmos. Ocean. Technol. **22:** 1797–1808.

Morris, A. W., and J. P. Riley. 1966. The bromide/chlorinity and sulphate/chlorinity ratio in sea water. Deep-Sea Res. **13:** 699–705.

Okubo, A. 1971. Oceanic diffusion diagrams. Deep-Sea Res. **18:** 789–802.

Osborn, T. R. 1980. Estimates of the local rate of vertical diffusion from dissipation measurements. J. Phys. Oceanogr. **10:** 83–89.

Pennington, J. T., and F. P. Chavez. 2000. Seasonal fluctuations of temperature, salinity, nitrate, chlorophyll and primary production at station H3/M1 over 1989–1996 in Monterey Bay, California. Deep-Sea Res. II **47:** 947–973.

Rosenfeld, L. K., F. B. Schwing, N. Garfield, and D. E. Tracy. 1994. Bifurcated flow from an upwelling center: A cold water source for Monterey Bay. Cont. Shelf Res. **14:** 931–964.

Ryan, J. P., F. P. Chavez, and J. G. Bellingham. 2005. Physical-biological coupling in Monterey Bay, California: Topographic influences on phytoplankton ecology. Mar. Ecol. Prog. Ser. **287:** 23–32.

———, and others. 2008. A coastal ocean extreme bloom incubator. Geophys. Res. Lett. **35:** L12602, doi:10.1029/2008GL034081.

Sakamoto, C. M., and others. 2004. Influence of Rossby waves on nutrient dynamics and the plankton community structure in the North Pacific subtropical gyre. J. Geophys. Res. **109:** C05032, doi:10.1029/2003JC001976.

———, F. J. Millero, W. Yao, G. E. Friederich, and F. P. Chavez. 1998. Surface seawater distributions of inorganic carbon and nutrients around the Galapagos Islands: Results from the PlumEx Experiment using automated chemical mapping. Deep-Sea Res. II **45:** 1055–1071.

Sarmiento, J. L., and N. Gruber. 2006. Ocean biogeochemical dynamics. Princeton Univ. Press.

Schlitzer, R. 2002. Carbon export fluxes in the Southern Ocean: Results from inverse modeling and comparison with satellite-based estimates. Deep-Sea Res. II **49:** 1623–1644.

———. 2007. Ocean Data View [Internet]. [accessed 5 December 2007]. Available from: http://odv.awi.de

Sibenac, M., W. J. Kirkwood, R. McEwen, F. Shane, R. Henthorn, D. Gashler, and H. Thomas. 2002. Modular AUV for routine deep water science operations. MTS-IEEE Proc. Oceans 2002 **1:** 167–172.

Statham, P. J., and others. 2005. Spatially complex distribution of dissolved manganese in a fjord as revealed by high-resolution in situ sensing using the autonomous underwater vehicle Autosub. Environ. Sci. Technol. **39:** 9440–9445.

Wankel, S. D., C. Kendall, J. T. Pennington, F. P. Chavez, and A. Paytan. 2007. Nitrification in the euphotic zone as evidenced by nitrate dual isotopic composition: Observations from Monterey Bay, California. Glob. Biogeochem. Cycles **21:** GB2009, doi:10.1029/2006GB002723.

Woodward, E. M. S., and A. P. Rees. 2001. Nutrient distributions in an anticyclonic eddy in the northeast Atlantic Ocean, with reference to nanomolar ammonium concentrations. Deep-Sea. Res. II **48:** 775–793.

Yu, X., T. Dickey, J. Bellingham, D. Manov, and K. Streitlien. 2002. The application of autonomous underwater vehicles for interdisciplinary measurements in Massachusetts and Cape Cod Bays. Cont. Shelf Res. **22:** 2225–2245.

Received: 31 August 2007
Accepted: 11 March 2008
Amended: 8 May 2008